

R4Det: 4D Radar-Camera Fusion for High-Performance 3D Object Detection

Zhongyu Xia¹ Yousen Tang^{1†} Yongtao Wang^{1✉} Zhifeng Wang² Weijun Qin²
¹ Wangxuan Institute of Computer Technology, Peking University ² EBTech Co. Ltd
 {xiazhongyu, wyt}@pku.edu.cn 2352614@tongji.edu.cn zhifengw@ebtech.com

Abstract

4D radar-camera sensing configuration has gained increasing importance in autonomous driving. However, existing 3D object detection methods that fuse 4D Radar and camera data confront several challenges. First, their absolute depth estimation module is not robust and accurate enough, leading to inaccurate 3D localization. Second, the performance of their temporal fusion module will degrade dramatically or even fail when the ego vehicle’s pose is missing or inaccurate. Third, for some small objects, the sparse radar point clouds may completely fail to reflect from their surfaces. In such cases, detection must rely solely on visual unimodal priors. To address these limitations, we propose R4Det, which enhances depth estimation quality via the Panoramic Depth Fusion module, enabling mutual reinforcement between absolute and relative depth. For temporal fusion, we design a Deformable Gated Temporal Fusion module that does not rely on the ego vehicle’s pose. In addition, we built an Instance-Guided Dynamic Refinement module that extracts semantic prototypes from 2D instance guidance. Experiments show that R4Det achieves state-of-the-art 3D object detection results on the TJ4DRadSet and VoD datasets.

1. Introduction

The cornerstone of autonomous driving safety lies in 3D perception. To achieve this goal, the community has been actively exploring sensor configurations that go beyond the conventional LiDAR-camera setup. Among emerging alternatives, 4D millimeter-wave radar has gained significant attention for its all-weather reliability, long-range sensing, and substantially lower cost compared with LiDAR. However, the inherent sparsity and noise characteristics of radar point clouds make it insufficient to support high-precision 3D detection on its own. Therefore, 4D radar-camera multi-modal fusion approaches have become the prevailing choice in practical applications. However, developing high-

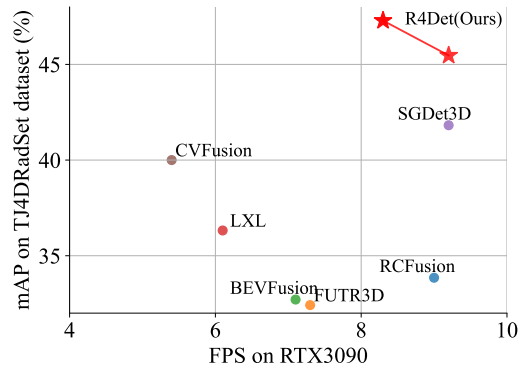


Figure 1. Comparison of R4Det with current 4D radar-camera real-time detectors.

performance 4D radar-camera 3D object detection models faces numerous challenges.

The primary challenge in current 4D radar-camera fusion frameworks is the limited accuracy of their absolute depth estimation module, which leads to inaccurate 3D localization. Current radar-camera fusion frameworks [1, 13, 14] rely on accurate dense depth estimation during view transformation. However, these methods only apply absolute depth supervision to foreground points, resulting in sparse depth supervision. Hence, they can not achieve high-quality panoramic depth estimation, which benefits foreground localization and reduces background noise. In addition, recent relative depth estimation works show strong generalization capabilities [2, 24, 26]. How to effectively leverage their capabilities for accurate panoramic absolute depth estimation is a topic worth investigating.

The second challenge confronting current radar-camera fusion frameworks involves temporal fusion due to the absence of the ego-vehicle pose. Temporal input provides crucial historical 3D information of occluded objects, which is essential for 3D object detection tasks. However, most methods developed upon the mainstream 4D radar dataset, *i.e.*, TJ4DRadSet, remain single-frame detectors, largely due to the lack of ego-vehicle pose in this dataset. Moreover, in real-world scenarios, particularly in rural areas, missing or inaccurate ego-vehicle poses due to GPS signal loss are also common. Hence, some studies [8] have begun

[†]This work was done as an intern at PKU. [✉]Corresponding author.

incorporating temporal information by merely stacking historical BEV features along the channel dimension, which yield limited improvements.

The third challenge lies in detecting small objects, *e.g.*, distant cyclists, which appear in the image without any point cloud reflected from their surfaces. For these challenging cases, it is necessary to leverage visual priors to identify them. Some works [6, 23] attempt to extract instance proposals from 2D features, but they all rely on Transformer-based architectures and regard the extracted instances only as queries, making them less compatible with other widely used CNN-based frameworks.

To address the three challenges mentioned above, we propose R4Det, a novel 4D radar-camera fusion framework for high-performance 3d object detection. To handle the first challenge, we propose the Panoramic Depth Fusion (PDF) module. Specifically, to eliminate geometric contamination, PDF abandons sparse metric regression and introduces a novel pairwise ordinal ranking loss with dynamic tolerance, enabling the model to learn high-fidelity, edge-sharp, and structurally continuous geometry. To tackle the second challenge, we design a Deformable Gated Temporal Fusion (DGTF) module that explicitly aligns non-rigid motion with deformable convolutions and smooths temporal noise through GRU-style gating, achieving stable feature aggregation without the instability of implicit recurrence. To deal with the third challenge, we propose an Instance-Guided Dynamic Refinement (IGDR) that leverages a 2D instance-guided semantic prototype to purify features, jointly optimized with the detection head to correct misprojected semantics and restore clarity for distant or partially occluded objects. To sum up, the key contributions of this work are:

- We present a 4D radar-camera detector for highly accurate, efficient, and robust 3D object detection.
- We propose three BEV-paradigm-compatible, plug-and-play modules, *i.e.*, Panoramic Depth Fusion, Deformable Gated Temporal Fusion, and Instance-Guided Dynamic Refinement, to produce high-quality panoramic absolute depth estimations, fuse temporal information without ego pose, and handle small objects, respectively.
- R4Det achieves state-of-the-art performance on both VoD and TJ4DRadSet dataset.

2. Related Work

2.1. Camera-only 3D Object Detection

Current camera-only 3D detection methods focus on reconstructing the 3D scene from synchronized image streams. BEVDet [5] and BEVDepth [11] predict dense pixel-wise depth maps and employ the Lift-Splat-Shoot (LSS) paradigm [18] to project image features into the bird’s-

eye-view (BEV) space, constructing dense BEV representations. Transformer-based methods, such as DETR3D [20] and PETR [15], use BEV queries or object-centric queries to perform implicit 2D-to-3D coordinate transformations and feature aggregation. Sparse geometry sampling strategies have also been explored to balance feature efficiency and spatial precision. To capture temporal information in dynamic scenarios, BEVFormer [12] and VideoBEV [4] integrate temporal information either in the BEV space or via recurrent feature fusion. Despite their rich semantic representations, camera-only systems still suffer from significant depth and geometric uncertainty under occlusion, illumination changes, or distant objects.

2.2. 4D Radar-Camera Fusion for 3D Object Detection

To overcome the limitations of camera-only perception and integrate robust geometric and motion information, 4D millimeter-wave radar-camera fusion has attracted significant attention. BEV-level fusion methods, such as CRN [8], use multi-modal deformable attention to align radar and camera BEV features, while HVDetFusion [10] and RCBEVDet [14] explore effective radar BEV feature extraction to supplement camera BEV streams. HyDRa [21] fuses features in both perspective and BEV spaces, CRAFT [7] introduces proposal-level fusion. RADIANT [16] leverages radar points to predict 3D offsets for correcting monocular depth errors without retraining the camera model. SGM3D [1] introduces a dual-branch fusion module and a localization-aware cross-attention to facilitate deep interactions across modalities. CVFusion [29] proposed Point- and grid-guided fusion modules to effectively fuse multiple-view features.

However, existing fusion detectors still face three challenges: (1) depth estimation heavily relies on sparse radar or LiDAR supervision, which induces geometric contamination with blurred boundaries and discontinuous structures; (2) temporal modeling is often simplified as naive feature concatenation, failing to align non-rigid motion effectively; (3) cumulative errors in geometric and modality alignment can contaminate BEV features, impairing instance separation and the detection of distant small objects.

3. Method

3.1. Overall Framework

As illustrated in Figure 2, the R4Det framework is a progressive purification pipeline designed to address three core challenges in 4D radar-camera object detection. First, using sparse radar features (extracted by the radar encoder) as queries, the **Panoramic Depth Fusion (PDF)** module establishes an accurate geometric foundation to extract dense image semantics (Sec. 3.2). The resulting image

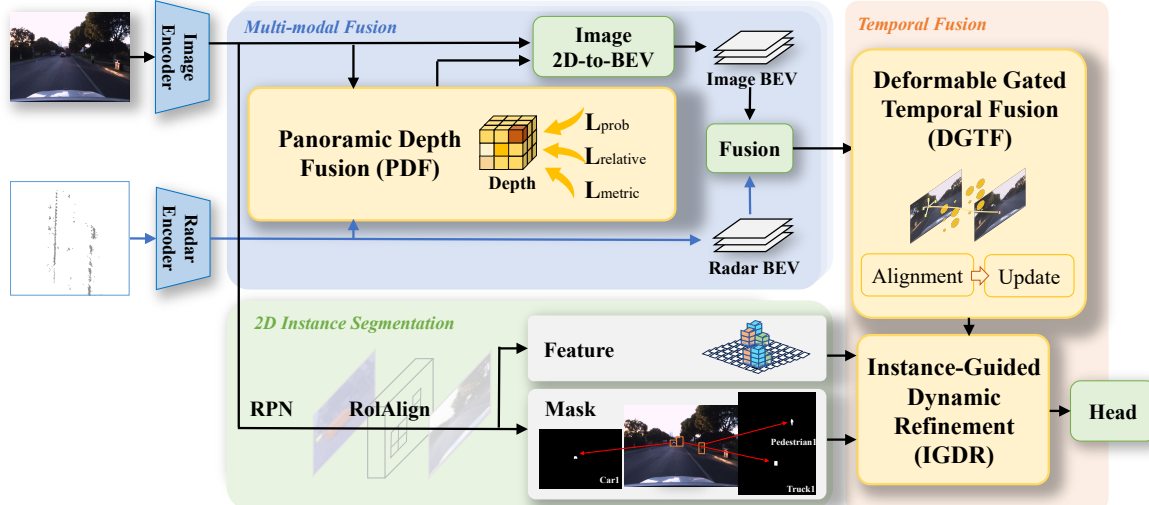


Figure 2. **Overall architecture of R4Det.** Our framework progressively purifies the BEV representation in three stages: i) The Panoramic Depth Fusion (PDF) module generates a geometrically-accurate BEV feature map from multi-modal inputs. ii) The Deformable Gated Temporal Fusion (DGTF) module performs pose-free alignment and integration to create a temporally consistent feature. iii) The Instance-Guided Dynamic Refinement (IGDR) module leverages 2D instance prototypes to purify the final features for 3D detection.

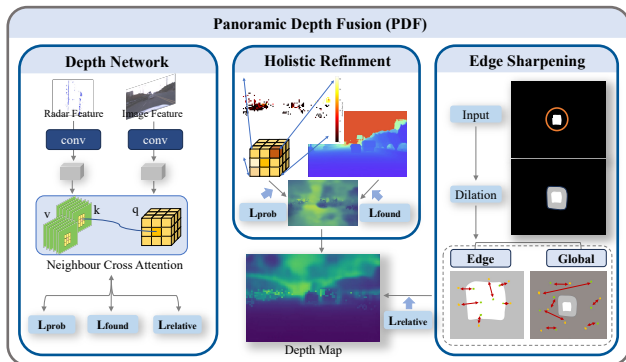


Figure 3. **Overview of the Panoramic Depth Fusion (PDF) module.**

BEV is then concatenated with the radar BEV via a *Multi-modal Fusion* block to produce an initial fused BEV feature map X_t . Next, our **Deformable Gated Temporal Fusion (DGTF)** module performs pose-free spatial alignment and gated updates on X_t to maintain a temporally consistent hidden state H_t and output a fused feature F_{RC} (Sec. 3.3). Finally, the **Instance-Guided Dynamic Refinement (IGDR)** module leverages 2D instance prototypes to dynamically calibrate F_{RC} , outputting a purified feature F_{final} to the 3D detection head (Sec. 3.4).

3.2. Panoramic Depth Fusion (PDF)

To establish a robust geometric foundation, we employ a Neighborhood Cross-Attention mechanism [1] to aggregate dense image semantics using sparse radar features as queries. Built upon this aggregated representation, we introduce a triplet of dedicated supervisions to fundamentally resolve depth ambiguity and geometric contamina-

tion. **Probabilistic Supervision.** We first supervise the predicted depth distribution $\mathcal{P} \in \mathbb{R}^{B \times D \times H \times W}$ using sparse high-precision LiDAR points d_g^{sparse} . Here, B is the batch size, D represents the number of depth bins, and H, W are the spatial dimensions of the BEV map. Specifically, each sparse point is converted to a Gaussian target distribution $\mathcal{G}(d_g^{\text{sparse}})$. Then, we minimize the KL divergence over sparse locations $\mathcal{M}_{\text{sparse}}$:

$$\mathcal{L}_{\text{prob}} = \frac{1}{|\mathcal{M}_{\text{sparse}}|} \sum_{i \in \mathcal{M}_{\text{sparse}}} \text{KL}(\mathcal{G}(d_{g_i}^{\text{sparse}}) \parallel \mathcal{P}_i). \quad (1)$$

This branch determines the network’s probabilistic output, ensuring that the ‘Splat’ operation in the subsequent view transformation is based on a sharp and accurate distribution, thereby preventing geometric scattering.

Foundation-Model-Guided Depth Supervision For the decoded expected depth map \hat{d} , we incorporate both sparse radar-anchored depth and dense pseudo-ground truth (Metric3D), denoted as d_g^{dense} , as supervision. By applying the Smooth L1 loss for both metric targets, we effectively prevent gradient explosion caused by potential radar outliers:

$$\mathcal{L}_{\text{found}} = \lambda_{\text{abs}} \mathcal{L}_{\text{abs}} + \lambda_{\text{dense}} \mathcal{L}_{\text{dense}}, \quad (2)$$

where

$$\mathcal{L}_{\text{abs}} = \frac{1}{|\mathcal{M}_{\text{sparse}}|} \sum_{i \in \mathcal{M}_{\text{sparse}}} \text{SmoothL1}(\hat{d}_i, d_{g_i}^{\text{sparse}}), \quad (3)$$

$$\mathcal{L}_{\text{dense}} = \frac{1}{|\mathcal{M}_{\text{dense}}|} \sum_{i \in \mathcal{M}_{\text{dense}}} \text{SmoothL1}(\hat{d}_i, d_{g_i}^{\text{dense}}). \quad (4)$$

This combination ensures both high metric precision on key points and robust structural coverage for the full scene.

Structural Ranking Supervision. To preserve local depth relationships, we adopt a relative depth ranking loss:

$$s_{ij} = \text{sign}(d_{g_i}^{\text{dense}} - d_{g_j}^{\text{dense}}), \quad (5)$$

$$\mathcal{L}_{\text{pair}}(i, j) = \text{Softplus}(-s_{ij}(\hat{d}_i - \hat{d}_j)). \quad (6)$$

However, naively sampling all pairs is inefficient, as most pairs lie on flat surfaces where small true depth differences are dominated by sensor noise, leading to ambiguous training signals. Therefore, we only select pixel pairs with a significant difference that exceeds their depth-dependent dynamic threshold given by:

$$\tau_{ij} = \max(\tau_{\text{abs}}, \tau_{\text{rel}} \cdot (d_{g_i}^{\text{dense}} + d_{g_j}^{\text{dense}})/2), \quad (7)$$

include pair if $|d_{g_i}^{\text{dense}} - d_{g_j}^{\text{dense}}| > \tau_{ij}$.

where τ_{abs} and τ_{rel} are the absolute and relative tolerance margins, respectively, designed to filter out noisy minor differences on flat surfaces. Furthermore, we apply a *foreground-biased dual sampling* strategy which separates edge regions and background:

$$\mathcal{L}_{\text{relative}} = w_{\text{edge}}\mathcal{L}_{\text{edge}} + w_{\text{global}}\mathcal{L}_{\text{global}}. \quad (8)$$

Here, w_{edge} and w_{global} are the balancing weights. $\mathcal{L}_{\text{global}}$ samples pixel pairs randomly from background regions, excluding foreground objects, to preserve overall scene structure. The core innovation lies in $\mathcal{L}_{\text{edge}}$'s *cross-boundary sampling*: we first dilate 2D instance masks to form a narrow *dilated ring* around each object (the difference between the dilated mask and original mask). During sampling, one pixel i is selected from this dilated ring (immediately outside the object), and the other j from the object's interior (original mask). This strategy forces the network to focus on sharp depth transitions at object boundaries, significantly enhancing contour sharpness and geometric accuracy.

Total Depth Loss. The overall depth loss combines all three supervisions is:

$$\mathcal{L}_{\text{depth}} = \lambda_1\mathcal{L}_{\text{prob}} + \lambda_2\mathcal{L}_{\text{found}} + \lambda_3\mathcal{L}_{\text{relative}}. \quad (9)$$

This depth loss encourages the network to generate depth maps that are probabilistically accurate, metric-scale precise, and structurally coherent, providing strong geometric priors for downstream 3D detection.

3.3. Deformable Gated Temporal Fusion (DGTF)

Fusing dense BEV features over time introduces two coupled challenges: *spatial misalignment* caused by ego-motion and object movement, and *temporal inconsistency* due to dynamic scene evolution. Conventional recurrent units try to address both issues jointly through a single gating mechanism, which is often inefficient and inaccurate when handling complex non-rigid motion. To address this

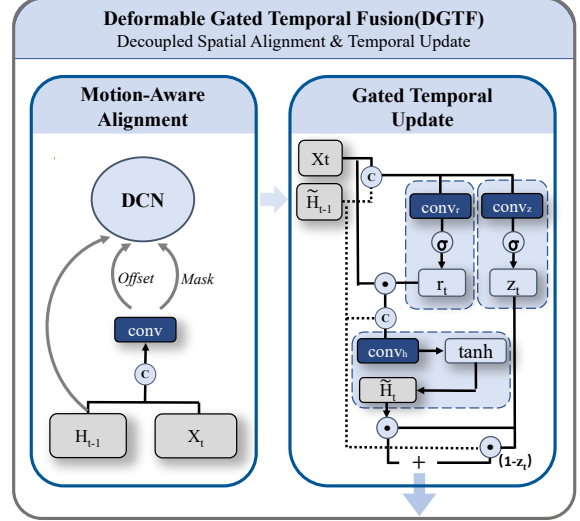


Figure 4. **Architecture of the proposed Deformable Gated Temporal Fusion (DGTF) module.** DGTF consists of two specialized branches: motion-aware alignment using deformable convolution and a gated temporal update mechanism.

Algorithm 1 Pseudo-code of Deformable Gated Temporal Fusion (DGTF)

-
- 1: **Input:** Current BEV feature X_t , previous hidden state H_{t-1}
 - 2: **Output:** Updated BEV feature H_t
 - 3: // *Motion-Aware Alignment*
 - 4: $(\Delta p, m) = \text{Conv}_{\text{offset}}(\text{Concat}(X_t, H_{t-1}))$
 - 5: $\tilde{H}_{t-1} = \text{DCNv2}(H_{t-1}, \Delta p, m)$
 - 6: // *Gated Information Update*
 - 7: $r_t = \sigma(\text{Conv}_r(\text{Concat}(X_t, \tilde{H}_{t-1})))$
 - 8: $\tilde{H}_t = \phi(\text{Conv}_h(\text{Concat}(X_t, r_t \odot \tilde{H}_{t-1})))$
 - 9: $z_t = \sigma(\text{Conv}_z(\text{Concat}(X_t, \tilde{H}_{t-1})))$
 - 10: $H_t = (1 - z_t) \odot X_t + z_t \odot \tilde{H}_t$
 - 11: $F_{RC} = \text{Conv}_{\text{out}}(H_t)$
 - 12: **return** F_{RC}
-

issue, we explicitly decouple the challenge into two problems and propose the Deformable Gated Temporal Fusion (DGTF) module with two branches, as illustrated in Figure 8. The motion-aware alignment branch addresses the spatial correction issue, while the gated temporal update branch addresses the feature evolution problem.

Motion-Aware Alignment Branch. Given the current BEV feature X_t and the previous hidden state H_{t-1} , we first predict the sampling offset Δp and modulation mask m through an offset prediction convolution:

$$\Delta p, m = \text{Conv}_{\text{offset}}(\text{Concat}(X_t, H_{t-1})). \quad (10)$$

The previous hidden feature is then aligned using deformable convolution (DCNv2):

$$\tilde{H}_{t-1} = \text{DCNv2}(H_{t-1}, \Delta p, m). \quad (11)$$

This step compensates for motion-induced spatial misalignment without ego-pose priors: the learned offsets Δp ex-

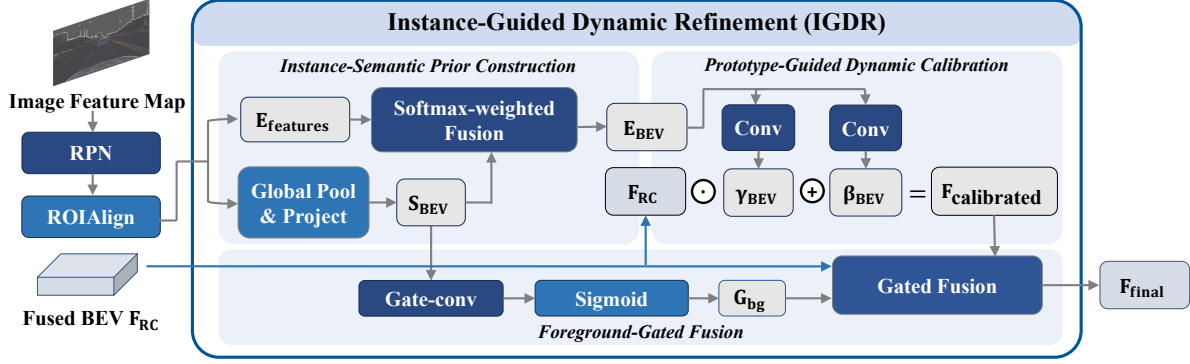


Figure 5. **Overview of Instance-Guided Dynamic Refinement (IGDR) module.** IGDR adaptively refines radar-camera BEV features by suppressing instance overlap contamination and cross-modality noise, while preserving reliable distant object representations.

explicitly reconstruct the relative motion flow, while the modulation mask m adaptively suppresses unreliable background regions, thereby producing geometrically consistent features across frames.

Gated Information Update Branch. After feature alignment, DGTF performs temporal reasoning via gated update units. The reset gate r_t estimates the relevance of the aligned historical feature:

$$r_t = \sigma(\text{Conv}_r(\text{Concat}(X_t, \tilde{H}_{t-1}))). \quad (12)$$

The candidate feature \tilde{H}_t integrates the filtered history and current observation:

$$\tilde{H}_t = \phi(\text{Conv}_h(\text{Concat}(X_t, r_t \odot \tilde{H}_{t-1}))). \quad (13)$$

Finally, the update gate z_t adaptively balances between new and historical information:

$$z_t = \sigma(\text{Conv}_z(\text{Concat}(X_t, \tilde{H}_{t-1}))), \quad (14)$$

$$H_t = (1 - z_t) \odot X_t + z_t \odot \tilde{H}_t. \quad (15)$$

where σ and ϕ denote the sigmoid and hyperbolic tangent (tanh) activation functions, respectively, and \odot represents the element-wise multiplication. The refined feature H_t is further processed by a lightweight convolutional layer (Conv_{out}) to produce the temporally aligned multi-modal feature F_{RC} for the subsequent module.

By disentangling spatial alignment and temporal update through ‘‘DCN for alignment, GRU for update’’, DGTF achieves fine-grained motion compensation and robust temporal consistency, leading to significantly improved dynamic perception in radar-camera BEV fusion.

3.4. Instance-Guided Dynamic Refinement (IGDR)

To address feature contamination in overlapping regions and blurred representations of distant small objects in BEV, we propose the Instance-Guided Dynamic Refinement (IGDR) module. The core idea is guidance: instead of relying on potentially noisy F_{RC} features to refine themselves,

we leverage parallel, clean 2D instance features as semantic priors to actively calibrate the main BEV feature stream.

Instance-Semantic Prior Construction. IGDR takes three inputs: the multi-modal BEV feature $F_{RC} \in \mathbb{R}^{B \times C \times H \times W}$ (from DGTF), 2D instance branch features $E_{features} \in \mathbb{R}^{N \times C_{inst} \times H' \times W'}$, and the instance spatial distribution map $S_{BEV} \in \mathbb{R}^{B \times N \times H \times W}$. Here, C denotes the channel dimension of the BEV map, N and C_{inst} represent the number of RPN instance proposals and their channel dimension, while H' and W' are the spatial resolutions of the 2D RoI features extracted by the 2D instance segmentation head. S_{BEV} serves as a spatial assignment map, representing the probability distribution of the N instances projected into the BEV space via LSS.

We first apply global average pooling over the spatial dimensions of $E_{features}$ and a projection layer to align channel dimensions, yielding instance prototype vectors $E_{proj} \in \mathbb{R}^{B \times N \times C_{inst}}$. Using S_{BEV} as a soft attention map, we broadcast the prototypes into the BEV space via *Softmax-weighted Fusion* to construct a clean instance feature map E_{BEV} :

$$A_{prob} = \text{Softmax}_{dim=N} \left(\frac{S_{BEV}}{\tau} \right), \quad (16)$$

$$E_{BEV} = \text{BMM}(A_{prob}, E_{proj}). \quad (17)$$

Here, τ is a temperature hyperparameter controlling the attention sharpness. $E_{BEV} \in \mathbb{R}^{B \times C_{inst} \times H \times W}$ represents the ideal instance semantics, fully decoupled from potential geometric projection errors and noise in F_{RC} .

Prototype-Guided Dynamic Calibration. The core innovation of IGDR is instance-guided dynamic calibration. Rather than directly fusing E_{BEV} with F_{RC} , we treat E_{BEV} as a conditional generator to predict a pair of affine transformation parameters (scale γ_{BEV} and bias β_{BEV}) for each spatial location via *Conv* layers:

$$\gamma_{BEV} = \text{Conv}_\gamma(E_{BEV}), \quad \beta_{BEV} = \text{Conv}_\beta(E_{BEV}) \quad (18)$$

We then apply a feature-wise affine transformation to the potentially noisy F_{RC} , producing the calibrated feature $F_{calibrated}$:

$$F_{calibrated} = F_{RC} \odot \gamma_{BEV} + \beta_{BEV} \quad (19)$$

This mechanism allows the clean instance semantics to actively *calibrate, enhance, or suppress* the main feature stream, effectively mitigating cross-instance contamination and improving the representation of distant small objects.

Foreground-Gated Fusion. To ensure calibration only affects instance regions while preserving background structure, we introduce a foreground gate G_{bg} . We first sum S_{BEV} along the instance dimension to represent the union of all instances, then apply a 3×3 Gate-conv layer followed by a *Sigmoid* function (σ) to generate a smooth gating map:

$$G_{bg} = \sigma \left(\text{Conv}_{gate} \left(\sum_{i=1}^N S_{BEV}^{(i)} \right) \right) \quad (20)$$

The final output is obtained via *Gated Fusion*:

$$F_{final} = (1 - G_{bg}) \odot F_{RC} + G_{bg} \odot F_{calibrated} \quad (21)$$

To prevent exposure bias during training, we strictly avoid using ground-truth bounding boxes to extract instance features. Instead, IGDR is trained using realistic, potentially imperfect proposals dynamically generated by the 2D detector. This simulated inference path forces the module to learn robust calibration under non-ideal priors, yielding a highly plug-and-play refinement block without modifying the backbone.

4. Experiments

4.1. Datasets and Metrics

We conduct experiments on two large-scale 4D radar-camera datasets: TJ4DRadSet [27] and View-of-Delft [17]. TJ4DRadSet provides data from diverse driving conditions

with four categories: *Car, Pedestrian, Cyclist, and Truck*. VoD offers data from complex urban traffic with three categories: *Car, Pedestrian, and Cyclist*. We follow the official evaluation protocols for both. For TJ4DRadSet, we report AP_{3D} and AP_{BEV} for targets within 70m. For VoD, we report two complementary metrics: AP_{EAA} (Entire Annotated Area) and AP_{DC} (Driving Corridor). A unified IoU threshold convention is used: 0.50 for *Car* and *Truck*, and 0.25 for *Pedestrian* and *Cyclist*.

4.2. Implementation Details

We train the model with a global batch size of 32 using a two-stage strategy identical to SGM3D [1]: (i) a 15-epoch spatial perception pretraining stage (freezing DGTF, IGDR, and the detection head) to initialize the PDF module and 2D instance branch for high-quality geometric and semantic priors; (ii) a 15-epoch spatial-temporal end-to-end finetuning stage with all parameters unfrozen to jointly optimize fusion, alignment, and dynamic refinement. We use AdamW with an initial learning rate of 4×10^{-4} and cosine decay, along with standard data augmentations including random flipping, rotation, and scaling. The data point on the right in Fig. 1 (mAP 45.47, FPS 9.2) reduced the channel numbers in its backbone and neck (256→224) to align its FPS with SGM3D.

4.3. Main Results

As shown in Table 1, R4Det significantly outperforms all existing methods across all categories on the challenging **TJ4DRadSet** dataset, which includes complex nighttime and overpass scenarios. Our framework improves upon the SGM3D [1] baseline by **+5.47%** and **+6.91%** in 3D and BEV mAP. It is worth noting that our method is effective for small objects, such as *Cyclist*, surpassing the previous best by a large margin of +7.91%. For the **VoD dataset**, as shown in Table 2, R4Det also demonstrate state-of-the-art performance. As shown in Figure 1 and Table 2, we conducted inference speed tests on a single 3090 GPU. The ex-

Table 1. Comparison of 3D object detection results on the test set of TJ4DRadSet [27]. In the modality column, R denotes 4D radar and C denotes camera. The best values are in bold.

Method	Modality	AP _{3D} (%)				mAP _{3D}	AP _{BEV} (%)				mAP _{BEV}
		Car	Pedestrian	Cyclist	Truck		Car	Pedestrian	Cyclist	Truck	
PointPillars [9]	R	21.26	28.33	52.47	11.18	28.31	38.34	32.26	56.11	18.19	36.23
CenterPoint [25]	R	22.03	25.02	53.32	15.92	29.07	33.03	27.87	58.74	25.09	36.18
RadarPillarNet [28]	R	28.45	26.24	51.57	15.20	30.37	45.72	29.19	56.89	25.17	39.24
SMURF [19]	R	28.47	26.22	54.61	22.64	32.99	43.13	29.19	58.81	32.80	40.98
RCFusion [28]	R+C	29.72	27.17	54.93	23.56	33.85	40.89	30.95	58.30	28.92	39.76
FUTR3D [3]	R+C	-	-	-	-	32.42	-	-	-	-	37.51
BEVFusion [13]	R+C	-	-	-	-	32.71	-	-	-	-	41.12
LXL [22]	R+C	-	-	-	-	36.32	-	-	-	-	41.20
SGM3D [1]	R+C	59.43	26.57	51.30	30.00	41.82	66.38	29.18	53.72	39.36	47.16
CVFusion [29]	R+C	51.54	29.49	49.41	29.55	40.00	58.07	31.65	51.29	35.29	44.07
R4Det	R+C	63.60	31.24	62.84	31.46	47.29	72.36	33.48	64.58	45.85	54.07

Table 2. Comparison of 3D object detection results on the val set of VoD [17]. R and C denote 4D radar and camera modalities, respectively. The best values are in bold.

Methods	Modality	Entire Annotated Area (AP _{EAA} , %)				Driving Corridor (AP _{DC} , %)				FPS
		Car	Pedestrian	Cyclist	mAP	Car	Pedestrian	Cyclist	mAP	
PointPillars [9]	R	37.06	35.04	63.44	45.18	70.15	47.22	85.07	67.48	113.9
CenterPoint [25]	R	32.74	38.00	65.51	45.42	62.01	48.18	84.98	65.06	-
RadarPillarNet [28]	R	39.30	35.10	63.63	46.01	71.65	42.80	83.14	65.86	98.8
SMURF [19]	R	42.31	39.09	71.50	50.97	71.74	50.54	86.87	69.72	-
RCFusion [28]	R+C	41.70	38.95	68.31	49.65	71.87	47.50	88.33	69.23	9.0
FUTR3D [3]	R+C	46.01	35.11	65.98	49.03	78.66	43.10	86.19	69.32	7.3
BEVFusion [13]	R+C	37.85	40.96	68.95	49.25	70.21	45.86	89.48	68.52	7.1
LXL [22]	R+C	42.33	49.48	77.12	56.31	72.18	58.30	88.31	72.93	6.1
SGDet3D [1]	R+C	53.16	49.98	76.11	59.75	81.13	60.91	90.22	77.42	9.2
CVFusion [29]	R+C	60.87	57.89	77.46	65.41	89.86	68.79	88.62	82.42	5.4
R4Det	R+C	66.90	55.42	77.75	66.69	90.62	66.47	93.96	83.68	8.3

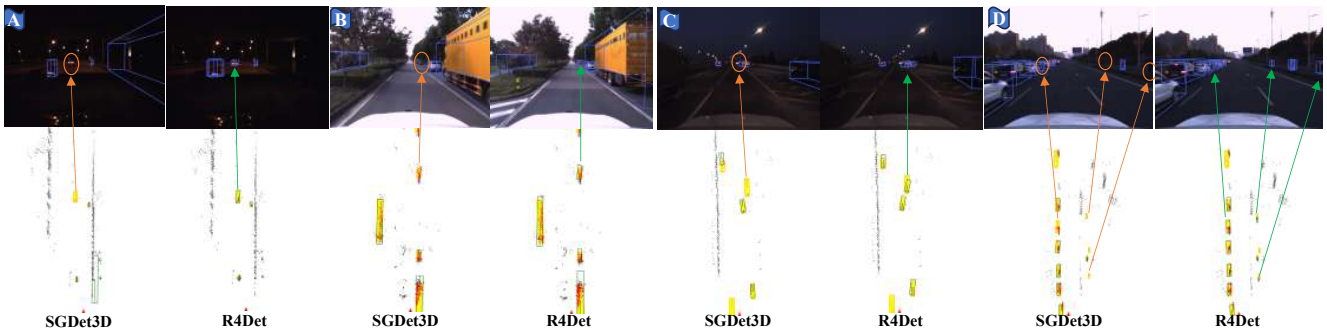


Figure 6. Example visualization results of R4Det and baseline on challenging scenarios (e.g., low-light conditions or small objects).

Table 3. More 3D object detection results on the val set of VoD to demonstrate the proposed modules are plug-and-play.

Method	Car	Pedestrian	Cyclist	mAP _{EAA}
BEVFusion [13]	37.85	40.96	68.95	49.25
BEVFusion + Ours	41.98	48.15	76.64	55.59
RCBEVDet [14]	40.63	38.86	70.48	49.99
RCBEVDet + Ours	41.02	48.85	76.12	55.33

perimental results demonstrate that R4Det achieves a better speed-accuracy balance.

We also applied the proposed module to BEVFusion [13] and RCBEVDet [14]. As shown in Table 3, our approach achieves improvements of +6.34% and +5.34% in mAP_{EAA}, respectively. This demonstrates the plug-and-play nature of our method.

4.4. Ablation

We conduct a chained ablation study on the TJ4DRadSet validation set [27]. As shown in Table 1, the first row presents the SGDet3D baseline. PDF enhances geometric perception through fine-grained depth completion (+1.71 mAP), DGTF strengthens temporal consistency via gated recurrent fusion (+3.55 mAP), and IGDR further refines BEV representations with instance-guided calibration

Table 4. Ablation study on each component of R4Det on the TJ4D Dataset.

PDF	DGTF	IGDR	mAP _{BEV}	mAP _{3D}	Car	Ped	Cyc	Truck
			45.15	39.86	58.67	25.93	47.89	26.24
✓			46.86	41.41	59.76	23.35	55.08	29.25
✓	✓		50.41	44.86	61.94	28.90	57.15	30.48
✓	✓	✓	54.07	47.29	63.60	31.24	62.84	31.46

(+3.66 mAP).

Effectiveness of the PDF Module. We evaluate the effectiveness of the Panoramic Depth Fusion module under a unified training configuration. The module uses four loss weights: λ_1 (0.1), λ_{abs} (0.01), λ_{dense} (0.03), and λ_3 (0.05). Different combinations correspond to different supervision configurations, as summarized in Table 5. Qualitative comparisons are provided in Figure 7. Our model maintains accurate depth and clear object boundaries under high-noise and low-light conditions, demonstrating strong generalization. Adding the metric loss (λ_{dense}) improves mAP from 45.15 to 46.08 (+0.93), while the relative loss (λ_3) further increases it to 46.86 (+0.78).

Effectiveness of the DGTF Module As shown in Table 6, we perform a set of step-wise ablation studies to validate the effectiveness of each component in the DGTF module. Adding simple feature concatenation (V1) already im-

Table 5. **Ablation of the Panoramic Depth Fusion module.** Each setting corresponds to different combinations of loss components.

Setting	λ_1	λ_{abs}	λ_{dense}	λ_3	BEV mAP \uparrow
A	0.1	0.01	–	–	45.15
B	0.1	0.01	0.03	–	46.08
C	0.1	0.01	0.03	0.05	46.86

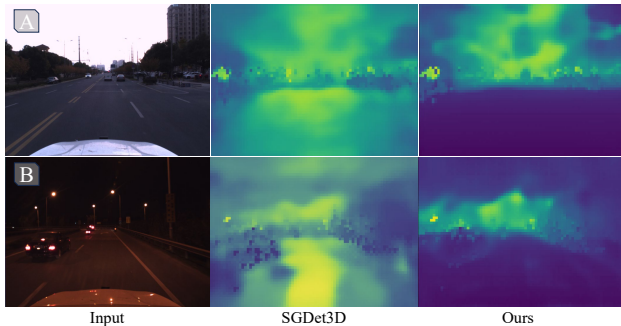


Figure 7. **Qualitative comparison of depth predictions by our Panoramic Depth Fusion and the baseline method.**

Table 6. **Ablation of the Deformable Gated Temporal Fusion module.** V1 (+Concat) concatenates current and previous BEV features; V2 (+DCN) adds modulated deformable convolution (DCNv2) to spatially align features; V4 (DGTF, Ours) further incorporates a GRU-style gating mechanism (ConvGRU) for selective temporal fusion; V3 (+SE) adds channel-wise Squeeze-and-Excitation on top of V4.

Variant	Concat	DCN	ConvGRU	SE	BEV mAP	3D mAP
V0					46.86	41.41
V1	✓				47.82	42.01
V2	✓	✓			48.86	43.32
V3	✓	✓	✓	✓	49.12	42.47
V4 (Ours)	✓	✓	✓		50.41	44.86

proves temporal consistency, while deformable alignment (V2) further enhances motion-aware fusion. Introducing the gating mechanism (ConvGRU) yields the largest gain (+3.45 3D mAP), confirming the importance of adaptive update and forgetting. Squeeze-and-Excitation brings no additional benefit, suggesting that ConvGRU already performs effective channel selection. Overall, DGTF (V4) enhances BEV localization by +3.55 mAP and 3D detection by +3.45 mAP, demonstrating robust and efficient temporal fusion.

Effectiveness of the IGDR Module To validate the effectiveness of each component in the proposed IGDR module, we conduct a comprehensive ablation study. Starting from a baseline that only uses the main BEV feature F_{RC} , we progressively build up to the full model. The results clearly demonstrate the evolution of our IGDR design: (1) *From baseline to prototype fusion (A \rightarrow B \rightarrow C)*: The baseline A (+PDF+DGTF), which directly uses the raw BEV features F_{RC} , achieves 50.41% mAP. Naively adding the Softmax-weighted prototype (B) yields limited gains, demonstrating that direct fusion introduces background noise. However, introducing the gating mechanism (C) to selectively fuse the foreground significantly improves performance to 51.60%

Table 7. **Ablation on the Instance-Guided Dynamic Refinement module.** *Gen.* indicates the generator used to produce calibration parameters or replacement maps. (1) **None (A)**: Baseline without refinement. (2) **Softmax-Fusion (B)**: Directly adds the Softmax-weighted instance prototype E_{BEV} to the main stream without gating. (3) **Static Map (C)**: Statically replaces the foreground region in F_{RC} with E_{BEV} under gating. (4) **MLP (D)**: Generates γ, β from E_{proj} using MLPs, followed by affine transformation. (5) **Attention (E)**: Employs a masked attention mechanism using F_{RC} as Query and E_{proj} as Key/Value. (6) **Conv (F, Ours)**: Constructs the spatial prototype E_{BEV} and generates γ, β via Conv2d layers, enabling spatially-aware calibration. Our convolutional generator achieves the best overall performance.

ID	Component		BEV mAP (%)		
	G_{bg}	Gen.	Cyclist	Pedestrian	Overall
A		None	57.51	31.66	50.41
B		Softmax-Fusion	58.14	32.00	51.29
C	✓	Static Map	58.62	31.92	51.60
D	✓	MLP	62.13	32.43	52.48
E	✓	Attention	62.21	32.21	52.52
F	✓	Conv	64.59	33.48	54.07

(+1.19 mAP over A). This confirms that gating is essential to filter out unreliable regions and provides a clean foundation for dynamic refinement. (2) *Necessity of dynamic calibration (C \rightarrow D)*: The MLP-based calibration (D) introduces instance-adaptive γ, β parameters from E_{proj} , leading to a further +0.88 mAP gain, validating the idea of calibrating rather than replacing F_{RC} . (3) *Choice of calibration generator (D \rightarrow E \rightarrow F)*: While the attention-based generator (E) provides marginal improvement (+0.04 mAP), our convolutional generator (F) achieves the best result (+1.55 mAP). The spatial-to-spatial mapping ($E_{BEV} \rightarrow F_{RC}$) via convolution captures local geometric patterns more effectively than non-spatial (MLP) or attention-based counterparts. Overall, the proposed IGDR achieves the highest performance (54.07 mAP, +3.66 over the baseline) and demonstrates a robust, efficient refinement mechanism for radar-camera BEV fusion.

5. Conclusion

In this paper, we present R4Det, a 4D radar-camera multi-modal 3D object detector for highly accurate, efficient, and robust 3D object detection. R4Det enhances depth estimation quality via the Panoramic Depth Fusion module, enabling mutual reinforcement between absolute and relative depth. For temporal fusion, we design a Deformable Gated Temporal Fusion module that does not rely on the ego vehicle’s pose. In addition, we built an Instance-Guided Dynamic Refinement module that extracts semantic prototypes from 2D instance guidance. Experiments show that R4Det achieves state-of-the-art 3D object detection results on both TJ4DRadSet and VoD datasets.

Acknowledgements

This work was supported by the National Natural Science Foundation of China (Grant No. 62176007).

References

- [1] Xiaokai Bai, Zhu Yu, Lianqing Zheng, Xiaohan Zhang, Zili Zhou, Xue Zhang, Fang Wang, Jie Bai, and Hui-Liang Shen. Sgdet3d: Semantics and geometry fusion for 3d object detection using 4d radar and camera. *RAL*, 2024. 1, 2, 3, 6, 7
- [2] Shariq Farooq Bhat, Reiner Birkl, Diana Wofk, Peter Wonka, and Matthias Müller. Zoedepth: Zero-shot transfer by combining relative and metric depth. *arXiv preprint arXiv:2302.12288*, 2023. 1
- [3] Xuanyao Chen, Tianyuan Zhang, Yue Wang, Yilun Wang, and Hang Zhao. Futr3d: A unified sensor fusion framework for 3d detection. In *CVPR*, 2023. 6, 7
- [4] Chunrui Han, Jinrong Yang, Jianjian Sun, Zheng Ge, Runpei Dong, Hongyu Zhou, Weixin Mao, Yuang Peng, and Xiangyu Zhang. Exploring recurrent long-term temporal fusion for multi-view 3d perception. In *RAL*, 2024. 2
- [5] Junjie Huang, Guan Huang, Zheng Zhu, Yun Ye, and Dalong Du. Bevdet: High-performance multi-camera 3d object detection in bird-eye-view. *arXiv preprint arXiv:2112.11790*, 2021. 2
- [6] Xiaohui Jiang, Shuailin Li, Yingfei Liu, Shihao Wang, Fan Jia, Tiancai Wang, Lijin Han, and Xiangyu Zhang. Far3d: Expanding the horizon for surround-view 3d object detection. In *AAAI*, 2024. 2
- [7] Youngseok Kim, Sanmin Kim, Jun Won Choi, and Dongsuk Kum. Craft: Camera-radar 3d object detection with spatio-contextual fusion transformer. In *AAAI*, 2023. 2
- [8] Youngseok Kim, Juyeb Shin, Sanmin Kim, In-Jae Lee, Jun Won Choi, and Dongsuk Kum. Crn: camera radar net for accurate, robust, efficient 3d perception. In *ICCV*, 2023. 1, 2
- [9] Alex H Lang, Sourabh Vora, Holger Caesar, Lubing Zhou, Jiong Yang, and Oscar Beijbom. Pointpillars: Fast encoders for object detection from point clouds. In *CVPR*, 2019. 6, 7
- [10] Kai Lei, Zhan Chen, Shuman Jia, and Xiaoteng Zhang. Hvdetfusion: A simple and robust camera-radar fusion framework. *arXiv preprint arXiv:2307.11323*, 2023. 2
- [11] Yinhao Li, Zheng Ge, Guanyi Yu, Jinrong Yang, Zengran Wang, Yukang Shi, Jianjian Sun, and Zeming Li. Bevdepth: Acquisition of reliable depth for multi-view 3d object detection. In *AAAI*, 2023. 2
- [12] Zhiqi Li, Wenhao Wang, Hongyang Li, Enze Xie, Chonghao Sima, Tong Lu, Yu Qiao, and Jifeng Dai. Bevformer: Learning bird’s-eye-view representation from multi-camera images via spatiotemporal transformers. In *ECCV*, 2022. 2
- [13] Tingting Liang, Hongwei Xie, Kaicheng Yu, Zhongyu Xia, Zhiwei Lin, Yongtao Wang, Tao Tang, Bing Wang, and Zhi Tang. Bevfusion: A simple and robust lidar-camera fusion framework. In *NeurIPS*, 2022. 1, 6, 7
- [14] Zhiwei Lin, Zhe Liu, Zhongyu Xia, Xinhao Wang, Yongtao Wang, Shengxiang Qi, Yang Dong, Nan Dong, Le Zhang, and Ce Zhu. Rcbvdet: Radar-camera fusion in bird’s eye view for 3d object detection. In *CVPR*, 2024. 1, 2, 7
- [15] Yingfei Liu, Tiancai Wang, Xiangyu Zhang, and Jian Sun. Petr: Position embedding transformation for multi-view 3d object detection. In *ECCV*, 2022. 2
- [16] Yunfei Long, Abhinav Kumar, Daniel Morris, Xiaoming Liu, Marcos Castro, and Punarjay Chakravarty. Radiant: Radar-image association network for 3d object detection. In *AAAI*, 2023. 2
- [17] Andras Palffy, Ewoud Pool, Srimannarayana Baratam, Julian FP Kooij, and Dariu M Gavrilă. Multi-class road user detection with 3+ 1d radar in the view-of-delft dataset. *RAL*, 2022. 6, 7
- [18] Jonah Philion and Sanja Fidler. Lift, splat, shoot: Encoding images from arbitrary camera rigs by implicitly unprojecting to 3d. In *ECCV*, 2020. 2
- [19] Austin Stone, Daniel Maurer, Alper Ayyaci, Anelia Angelova, and Rico Jonschkowski. Smurf: Self-teaching multi-frame unsupervised raft with full-image warping. In *CVPR*, 2021. 6, 7
- [20] Yue Wang, Vitor Guizilini, Tianyuan Zhang, Yilun Wang, Hang Zhao, and Justin Solomon. Detr3d: 3d object detection from multi-view images via 3d-to-2d queries. In *CoRL*, 2021. 2
- [21] Philipp Wolters, Johannes Gilg, Torben Teepe, Fabian Herzog, Anouar Laouichi, Martin Hofmann, and Gerhard Rigoll. Unleashing hydra: Hybrid fusion, depth consistency and radar for unified 3d perception. In *ICRA*, 2025. 2
- [22] Weiyi Xiong, Jianan Liu, Tao Huang, Qing-Long Han, Yuxuan Xia, and Bing Zhu. Lxl: Lidar excluded lean 3d object detection with 4d imaging radar and camera fusion. *IEEE TIV*, 2023. 6, 7
- [23] Chenyu Yang, Yuntao Chen, Hao Tian, Chenxin Tao, Xizhou Zhu, Zhaoxiang Zhang, Gao Huang, Hongyang Li, Yu Qiao, Lewei Lu, et al. Bevformer v2: Adapting modern image backbones to bird’s-eye-view recognition via perspective supervision. In *CVPR*, 2023. 2
- [24] Lihe Yang, Bingyi Kang, Zilong Huang, Xiaogang Xu, Jiashi Feng, and Hengshuang Zhao. Depth anything: Unleashing the power of large-scale unlabeled data. In *CVPR*, 2024. 1
- [25] Tianwei Yin, Xingyi Zhou, and Philipp Krahenbuhl. Center-based 3d object detection and tracking. In *CVPR*, 2021. 6, 7
- [26] Wei Yin, Chi Zhang, Hao Chen, Zhipeng Cai, Gang Yu, Kaixuan Wang, Xiaozhi Chen, and Chunhua Shen. Metric3d: Towards zero-shot metric 3d prediction from a single image. In *ICCV*, 2023. 1
- [27] Lianqing Zheng, Zhixiong Ma, Xichan Zhu, Bin Tan, Sen Li, Kai Long, Weiqi Sun, Sihan Chen, Lu Zhang, Mengyue Wan, et al. Tj4dradset: A 4d radar dataset for autonomous driving. *IEEE ITSC*, 2022. 6, 7
- [28] Lianqing Zheng, Sen Li, Bin Tan, Long Yang, Sihan Chen, Libo Huang, Jie Bai, Xichan Zhu, and Zhixiong Ma. Rcfusion: Fusing 4-d radar and camera with bird’s-eye view features for 3-d object detection. *IEEE TIM*, 2023. 6, 7

- [29] Hanzhi Zhong, Zhiyu Xiang, Ruoyu Xu, Jingyun Fu, Peng Xu, Shaohong Wang, Zhihao Yang, Tianyu Pu, and Eryun Liu. Cvfusion: Cross-view fusion of 4d radar and camera for 3d object detection. In *ICCV*, 2025. [2](#), [6](#), [7](#)

R4Det: 4D Radar-Camera Fusion for High-Performance 3D Object Detection

Supplementary Material

A. Additional ablation of the PDF module

Table 8 further presents the experimental process of adjusting the loss weight of the PDF module. Sensitivity analysis (C1–C4) shows that slight variations of λ_1 , λ_3 , λ_{dense} , or λ_{abs} lead to minor performance drops, confirming that the final setting (C5) achieves a balanced trade-off between stability and accuracy.

Table 8. **Ablation of the Panoramic Depth Fusion module.** Each setting corresponds to different combinations of loss components.

Setting	λ_1	λ_{abs}	λ_{dense}	λ_3	BEV mAP \uparrow
A	0.1	0.01	–	–	45.15
B (+ λ_{dense})	0.1	0.01	0.03	–	46.08
C1 ($\downarrow\lambda_1$)	0.05	0.01	0.03	0.05	46.64
C2 ($\downarrow\lambda_3$)	0.1	0.01	0.03	0.02	46.30
C3 ($\uparrow\lambda_{\text{dense}}$)	0.1	0.01	0.05	0.05	46.45
C4 ($\uparrow\lambda_{\text{abs}}$)	0.1	0.03	0.03	0.05	46.12
C5 (ours)	0.1	0.01	0.03	0.05	46.86

B. Additional ablation of the DGTF module

We also examine temporal depth sensitivity (Table 9): using the immediate predecessor ($t-1$) achieves the best accuracy and stability, whereas fusing more distant frames ($t-2$, $t-3$) leads to noise accumulation.

Table 9. **Sensitivity to historical frame gap.** Evaluation of different historical fusion depths. Single-step ($t-1$) achieves the best accuracy and stability.

Fusion Depth	BEV mAP	3D mAP
t & $t-3$	49.20	42.74
t & $t-2$	49.87	43.12
t & $t-1$	50.41	44.86

C. Qualitative Analyses of the DGTF module

R4Det is the first to validate the feasibility of temporal modeling on these two datasets. As shown in the Figure 8, the learned offsets Δp (red arrows) can align with object motion, reconstructing relative motion flow, while the mask m precisely suppresses the background. This physically proves DGTF performs explicit, physics-based motion alignment.

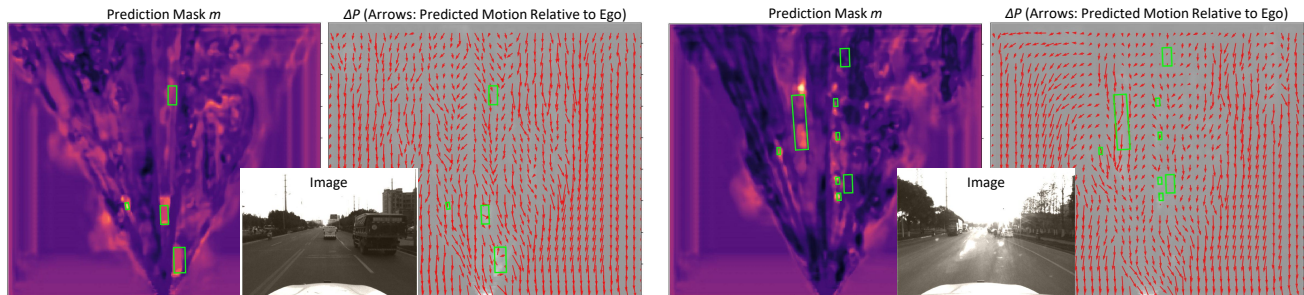


Figure 8. **DGTF Visualization.** Learned offsets (Δp , red arrows) align strictly with vehicle motion, while the mask (m , heatmap) suppresses background, proving explicit temporal alignment.